Research Article | Vol. 28, No. 4 / 17 February 2020 / Optics Express 4801
Optics EXPRESS

Extended cavity quantum cascade laser with cavity resonator integrated grating filter

S. Augé,[1] S. Gluchko,[2] A. L. Fehrembach,[3] E. Popov,[3] T. Antoni,[4] S. Pelloquin,[1] A. Arnoult,[1] G. Maisons,[5] A. Monmayrant,[1,*] and O. Gauthier-Lafaye[1]

[1]*LAAS-CNRS, Université de Toulouse, CNRS, Toulouse, France*
[2]*Laboratoire EM2C, CNRS, CentraleSupélec, Université Paris-Saclay, 3, rue Joliot Curie, 91192 Gif-sur-Yvette cedex, France*
[3]*Aix-Marseille Univ, CNRS, Centrale Marseille, Institut Fresnel, Marseille, France*
[4]*Université Paris-Saclay, CNRS, ENS Paris-Saclay, CentraleSupélec, LuMIn, 91190, Gif-sur-Yvette, France*
[5]*mirSense, 8 Av. de la Vauve, 91120 Palaiseau, France*
[*]*antoine.monmayrant@laas.fr*

Abstract: We report on an extended cavity quantum cascade laser based on a cavity resonator integrated grating filter (CRIGF) that acts as both cavity end-reflector and spectral selector. Stable, mode-hop free, single-mode emission around 2150 cm^{-1} is obtained over large injection current ranges (more than 50 mA) with a typical threshold around 290 mA. A digital frequency tuning over more than 65 cm^{-1} is obtained by changing the periodicity of the CRIGF ending the extended cavity.

© 2020 Optical Society of America under the terms of the OSA Open Access Publishing Agreement

1. Introduction

Tunable mid-infrared lasers are of high interest for many spectroscopic applications such as gas sensing, environment monitoring and so on [1]. External Cavity Quantum Cascade Lasers (EC-QCLs) have been demonstrated years ago and are now well established for such applications [2]. They rely on intra-cavity optical feedback using a grating in either Littrow or Littman configurations. This implementation is one of their main remaining limitation: since the tuning is achieved through a rotation of the grating, the wavelength repeatability is limited by the angular control of the grating. In this paper, we report on an alternative design of EC-QCLs where the optical feedback is produced by a sub-wavelength pixelated optical reflective filter called Cavity Resonator Integrated Grating Filter (CRIGF) [3].

As seen on Fig. 1, these reflective filters were made on a GaAs substrate with a 5.61 μm-thick $Al_{0.9}Ga_{0.1}As$ insulation layer and a 2.04 μm-thick GaAs waveguide. Three different gratings are etched in this waveguide: a Grating Coupler (GC) of period Λ_{GC} with here 31 periods, and 2 Distributed Bragg Reflectors (DBR) of period $\Lambda_{DBR} = \Lambda_{GC}/2$. Basically, the GC act as an input grating coupler into a cavity mode localized in the waveguide and delimited by the 2 DBRs, resulting in a sharp reflectance peak at the resonant wavelength which is fixed by the grating period Λ_{GC}.

These filters exhibit highly interesting properties, such as narrow-bandwidth reflectivity with high angular tolerance [4], gradient-based tunability [5] and have already been used to setup external cavities for near infrared laser diodes [6]. The paper is organized as follow. We first describe the external cavity setup and its alignment procedure. We then report on the experimental output power and threshold, before investigating in detail the spectral tuning and spectral stability of the cavity.

#385740 https://doi.org/10.1364/OE.385740
Journal © 2020 Received 13 Dec 2019; revised 24 Jan 2020; accepted 25 Jan 2020; published 5 Feb 2020

Optics EXPRESS

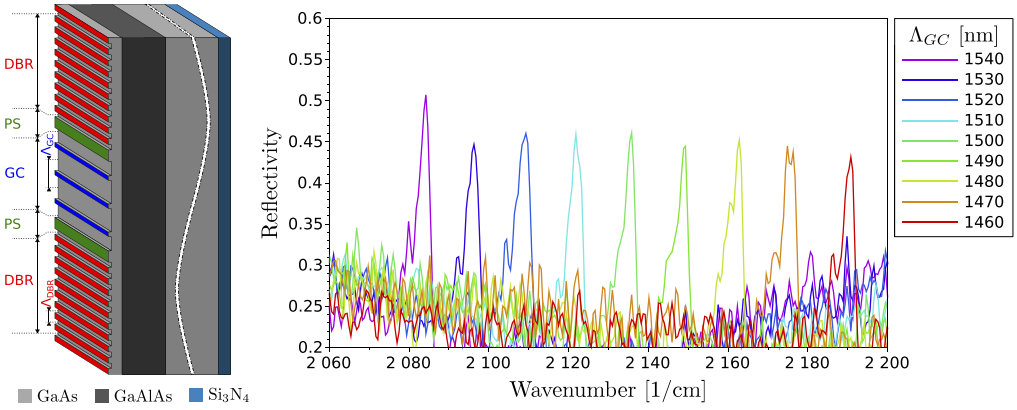

Fig. 1. (left) Schematic of a MIR CRIGF structure; (right) Reflectivities measured by FTIR microscopy on a sample similar to the one used here, for different base GC periods Λ_{GC}.

2. Extended cavity geometry and alignment

2.1. Cavity components

The geometry of the extended cavity is as reported in [6]. It consists of a cat's-eye configuration external cavity (see Fig. 2), that provided high robustness towards vibrations [7].

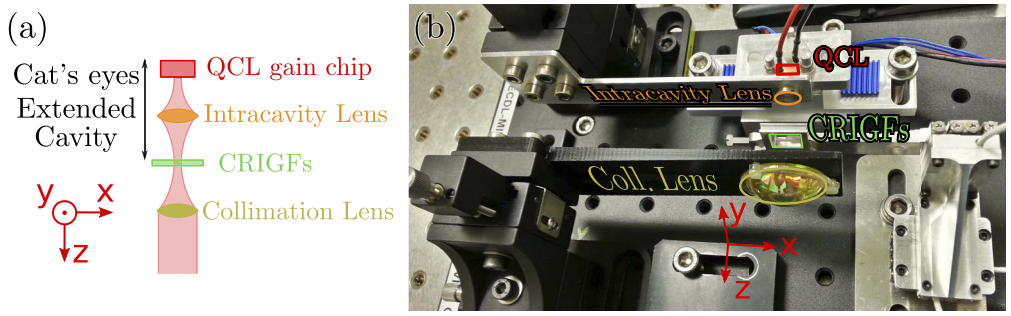

Fig. 2. (a) schematic of the cat's-eye quantum cascade extended cavity; (b) corresponding top view.

It contains only three elements: a QCL gain chip, an intra-cavity lens and a sample with several different CRIGFs.

The QCL chip (in red in Fig. 2) is of standard conception, using strain-compensated AlInAs/InGaAs heterostructures on InP where 6-μm-wide and 4-mm-long ridge waveguides are defined. The devices are mounted epi-side down on an AlN submount. The devices are High Reflectivity (HR) coated on the back facet. With an as cleaved front facet, these devices typically emit more than 100 mW CW at room temperature, with a threshold of around 280 mA, and a spectral gain between 2100 to 2200 cm^{-1} ([4.76 – 4.54] μm) with a maximum around 2165 cm^{-1}. For our experiments, the chips were Anti-Reflection (AR) coated on the front facet using a bi-layer SiO_2/TiO_2 coating. With this coating, the reflectivity of the front facet is sufficiently low to inhibit laser action of the QCL chip, turning it into a gain chip.

The intracavity lens (in orange in Fig. 2) is a high-numerical aperture aspheric lens with short focal length, AR-coated in the 3-5 μm range (Thorlabs C037TME-E). It images the mode emitted

Optics EXPRESS

at the AR facet of the QCL onto one of the CRIGF present on the sample (in green in Fig. 2) serving as an end-reflector in a simplified cat's-eye configuration.

The CRIGFs sample is held by a 3-axis motorized stage for precise overlapping of the image of the mode with the central part of one of the CRIGFs. The sample itself is fabricated as described in [8], with a single-layer Si_3N_4 antireflection coating on the backside of the substrate. In the wavelength range emitted by the QCL, the vertical multistack of the sample acts as both a planar waveguide and an AR-coating on the top side. The top layer of the stack is partially etched to define several CRIGFs with varying geometrical parameters (see [8] for details on the geometry and fabrication): the base period of the CRIGF, the filling factor of the central grating coupler (GC) and the filling factor of the side DBRs.

The performances of the CRIGFs are reported in [8]. For clarity, we summarize here the main properties of the sample we used. The base period of the CRIGF ranges from 1480 to 1560 nm, and linearly tunes the wavelength of the reflected peak around 2150 cm^{-1}. The peak reflectivity was measured to be around 40 %, with a large uncertainty ($\simeq$ 10 %). The filling factor of the GC, ranging from 45 % to 70 %, mainly impacts the peak reflectivity. The filling factor of the side DBRs (40 % or 45 %) impacts the efficiency of the DBRs and thus the overall efficiency of the filter. An optimum should be reached when critical coupling condition is achieved between the incoming laser spot and the planar Fabry-Pérot cavity formed by the waveguide and the side DBRs.

2.2. Cavity alignment

The sample contains 120 different CRIGFs that can be individually aligned with the image of the laser mode emitted from the AR facet of the QCL. For NIR wavelengths, this alignment is trivially achieved by re-imaging the image plane of the intracavity lens onto a cheap CMOS camera and by visually overlapping the GC of one CRIGF with the laser spot image [6]. This approach is not possible here. First, the direct imaging of the filter is quite challenging. Indeed, in the wavelength range of emission of the present QCL, available cameras are both expensive and offer low spatial resolution ruling out a direct observation of the mode/CRIGF overlap.

Second, contrary to standard semiconductor gain chips that emit a measurable amount of ASE (amplified spontaneous emission) in the absence of optical feedback, the QCL emission can not be easily detected in the spontaneous emission regime : in the absence of CRIGF to end the cavity, we injected current up to 450 mA without observing any emission. We thus set up an original alignment procedure based on indirect observation via feedback monitoring with the gain chip itself, benefiting from the large feedback sensitivity of QCL lasers below threshold [9]. Similarly to Self Mixing (SM) techniques, the gain chip is used both as an emitter and a detector. We thus inject a constant current in the QCL and monitor the voltage between its contact as a function of the position of the sample.

Figure 3 shows how this voltage evolves when scanning the position of the sample along the optical axis, for an injection current of I = 320 mA. A clear drop of nearly 70 mV is observed when the sample is in the image plane of the intracavity lens (z = 0). This can be explained as follows: when the sample gets closer to the image plane, more photons are fed-back into the QCL, thus changing the intracavity photon density which affects the carrier density and the voltage.

This first scan thus allows to precisely position the sample inside the image plane resulting in a 4.2-cm-long extended cavity.

The next step is to overlap one of the CRIGF with the optical beam. As shown on Fig. 4 this can also be achieved by recording the QCL voltage as a function of the (x, y) position in the image plane. Similarly to [10], we thus obtain an image of the optical reflectivity of our CRIGF sample.

In Fig. 4, we can clearly observe all the 120 CRIGFs and various labels and defects with great details. The 120 CRIGFs are arranged in two 10×6-matrices. The top one has a filling factor of 40 % for the DBRs, the bottom one 45 %. Within each matrix the GC filling factor ranges

Optics EXPRESS

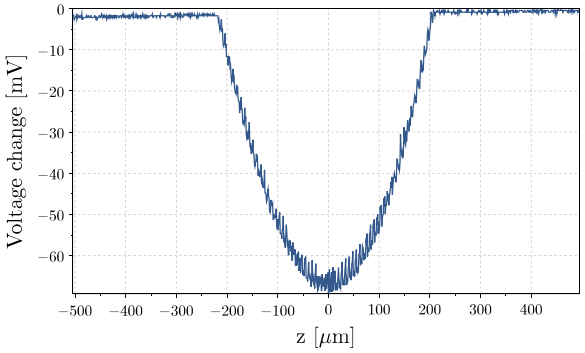

Fig. 3. Change in the voltage V between QCL contacts for a fixed injection current of $I = 320\,\text{mA}$ as a function of the position of the sample along the optical axis. $z = 0$ corresponds to the image plane where the bias voltage reaches a minimum.

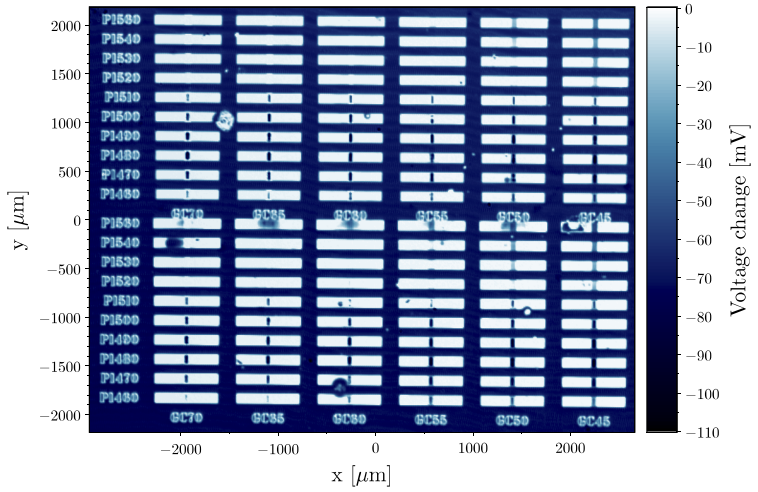

Fig. 4. Change of the voltage V between QCL contacts for a fixed injection current of I= 320 mA as a function of the (x, y) position of the sample in the image plane of the QCL facet. The different CRIGFs are clearly visible (large white rectangles arranged on two 6×10 matrices with varying geometrical parameters). CRIGFs where the central GC appears as a dark narrow vertical stripe are the one inducing the highest optical feedback in the QCL. They correspond to the CRIGFs spectrally matched with the QCL gain medium and able to stabilize the emitted frequency.

horizontally from 70 % to 45 % from left to right and the period ranges vertically from 1480 to 1560 nm. The CRIGFs appear as elongated white rectangles, some of them with a dark narrow stripe in the center. These dark stripes correspond to the central GCs. They correspond to the area on the sample effectively providing a spectrally selective reflection. Latter systematic tests of each CRIGF showed that the presence of this central dark stripe is a clear indicator that the spectral reflectivity of the CRIGF is within the gain region of the QCL and is thus able to provide spectral stabilization.

We thus have developed an alignment strategy that can easily determine the optimum positioning of the CRIGF in the cavity, together with a first indication of the good spectral matching of the CRIGF with the gain medium. It should be noted that this alignment protocol only ensures a spatial overlap of the facet emission spot with the CRIGF under study, but does not ensure that

Optics EXPRESS

the emission spot size matches the size of the GC of the CRIGF in the cavity. As shown in [4], the peak reflectivity of the CRIGF depends on this size matching, and larger optical feedback might be achieved after careful optimization of the intracavity magnification.

3. External cavity performances

After initial alignment, the external cavity setup emission versus current shows a clear signature of laser emission : abrupt threshold in the total emitted power at a given current, and narrow-band emission as measured by FTIR spectrometry. In this section, we discuss the performances achieved in terms of spectral emission and threshold current.

We measured the emitted spectrum as a function of the CRIGF period, focusing on the GC filling factor of 45 %. Figure 5 shows the emitted spectrum as a function of the CRIGF period for an injection current of $I = 340$ mA. The spectra were measured by a FTIR and the total emitted power by a thermopile powermeter.

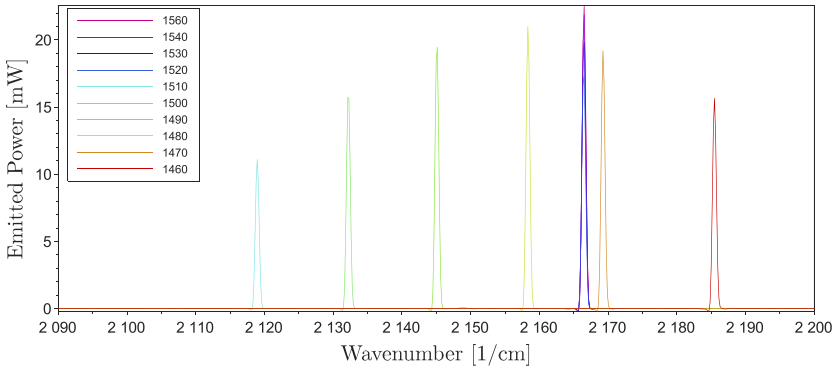

Fig. 5. Evolution of the emitted spectrum as a function of the GC period for a GC filling factor of 45 %. The vertical axis is normalized to the total emitted power.

For periods between 1460 and 1510 nm, the spectrum is locked to the peak reflectivity of the CRIGF, whereas for periods above 1510 nm, the spectrum is peaked somewhere near the maximum gain of the QCL.

Figure 6 summarizes the emitted power and peak wavenumber as a function of the CRIGF periodicity: we are able to digitally tune the emission of the QCL over 65 cm^{-1}, with a good linearity for GC periods between 1460 and 1510 nm. At the same time, the total emitted power varies between 11 and 22 mW. To further confirm that these performances stem from the spectral scanning of the gain curve of the gain chip by the wavelength imposed by the CRIGF filter, we then investigated the laser emission threshold as a function of the CRIGF used. As CRIGFs from the upper and lower matrices shown in Fig. 7 gave similar results, we only report here results obtained with the top ones, corresponding to a DBR filling factor of 40 %.

Figure 7 depicts the evolution of the thresholds with the CRIGF period for several filling factors of the GC. Typical thresholds are around 290 mA and an optimum is clearly visible for a GC period of 1480 nm, where the spectral overlap of the CRIGF reflectivity matches the peak of the gain in the QCL, as seen from the above spectra. In good agreement also, the threshold increases when the wavelength is tuned away from the gain peak. Thresholds also decrease for smaller filling factors, the best result being obtained for a filling factor of 45 %. This is in good agreement with independent CRIGFs characterization showing increasing peak reflectivities for smaller filling factors (see [8]). Even lower thresholds might be achievable using filling factors below 45 %.

Optics EXPRESS

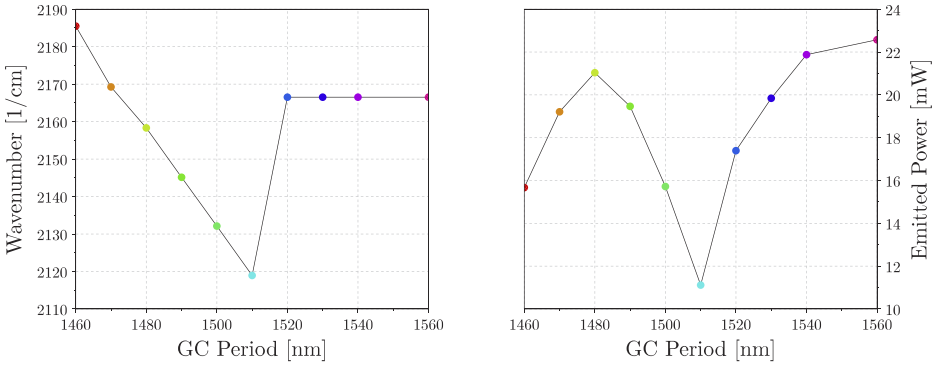

Fig. 6. Evolution of peak wavenumber and emitted power with the CRIGF periodicity.

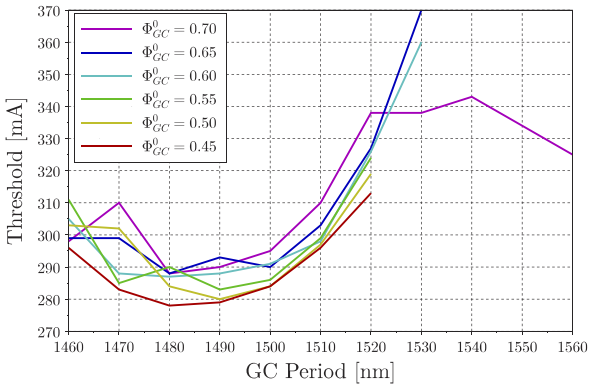

Fig. 7. Evolution of the lasing thresholds as a function of the GC period and coded filling factor Φ^0_{GC}.

4. Digital tuning and fine tuning of the cavity

4.1. *Digital tuning*

As seen, using several CRIGFs on a motorized stage allows to digitally tune the emission wavelength of the cavity by changing the sample position in front of the gain chip. To investigate the repeatability of this digital tuning, we registered the 7 positions of each of the CRIGFs providing good spectral stabilization and scan them sequentially repeating the scan 30 times (see Fig. 8 left). For these experiments, the injected current is always on, and kept constant at 330 mA. We used the CRIGFs with 40 % DBR filling factor and Φ^0_{GC} = 70 % and GC periods from 1460 nm to 1520 nm providing controlled emission in the 2108 - 2190 cm^{-1} range. For each position, we record a single spectra from the FTIR spectrometer.

From these measurements, and for each CRIGF, we have calculated the peak wavenumber obtained for each of the 30 passes and the deviation of this spectral position (with respect to the average wavenumber) is reported in Fig. 8 right. Each color corresponds to a different CRIGF.

We can observe some mode jumps (for CRGIF periods of 1520 and 1460 nm respectively in purple and red), that can be explained by thermal and mechanical changes in the cavity over the ~1-hour duration of the scan. Despite that, the spectral deviation stays way below 0.2 cm^{-1} for each CRIGF. This short term reproducibility is a major advantage of CRIGF based EC-QCL cavities as compared to grating based cavities. Indeed, the tuning is controlled via

Optics EXPRESS

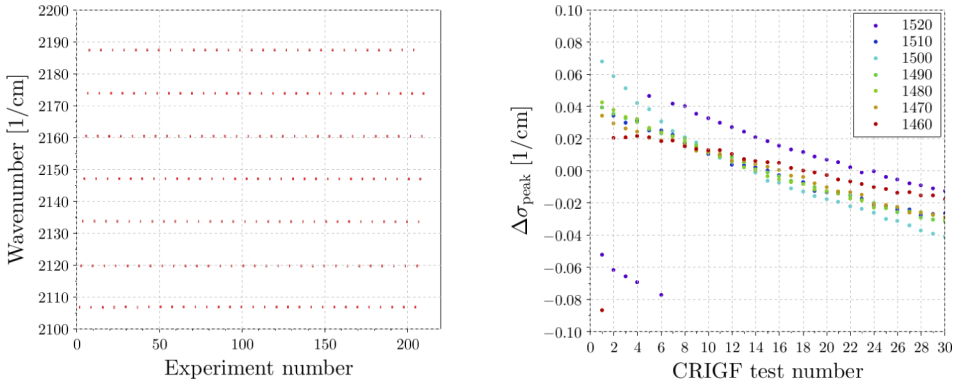

Fig. 8. Left : emitted spectrum as a function of the registered position while scaning 30 times over the 7 CRIGFs providing spectral stabilization. Right : change of peak wavenumber σ_{peak} during the scan presented in left figure. Each color corresponds to one CRIGF (GC period in the legend caption). The indicated change is relative to the average wavenumber over the scans for each CRIGF.

linear translations with a much simpler and better control than the rotations used in grating based external cavities.

4.2. Single-mode emission and mode-hopes

For a given CRIGF, the emission wavenumber can be finely tuned by the cavity length, where the phase condition for laser oscillation causes a wavenumber shift across the reflectivity spectrum of the CRIGF filter. Figure 9 left shows the wavenumber evolution with the cavity length when using a CRIGF with a 1480 nm period. We can observe smooth linear shift of the wavenumber with abrupt jumps every $\Delta Z \simeq 1.2\ \mu$m, the wavenumber excursion not exceeding 0.5 cm^{-1}. This shows that over a distance ΔZ the cavity is single-mode.

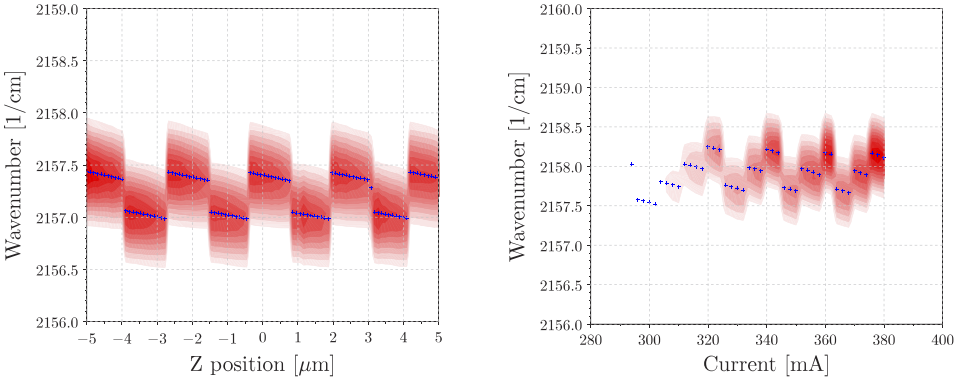

Fig. 9. Left : evolution of the spectra (color map, white to red, linear scale in arbitrary units) for increasing length of the cavity for the CRIGF with best overlap with the gain (1480 nm period). The injected current was 340 mA. The peak wavenumbers are reported as blue crosses for each acquired spectra. Right : evolution of the spectra with the injected current, for the same CRIGF, with the same conventions as left figure.

However, this signal differs from the saw-tooth pattern obtained when scanning the length of an ideal Fabry-Pérot cavity. This indicates that our cavity is perturbed by a parasitic sub-cavity. Indeed, a closer inspection of the mode hops reveals two alternating mode-hops of 0.31 cm^{-1}

Optics EXPRESS

and 0.45 cm^{-1}. This latter value of 0.45 cm^{-1} is in good agreement with a parasitic Fabry-Pérot cavity within the substrate of our filters (a 650-μm-thick GaAs with an optical index of 3.33 results in a free spectral range of 0.46 cm^{-1}).

Similarly, changing the current in the gain chip provides a small modification of the total optical cavity length, and allows a small tuning of the emission wavenumber, as depicted on Fig. 9 right. Increasing the current from the threshold to 380 mA, the wavenumber exhibits sharp mode hopes, the total excursion staying within 1 cm^{-1}. These two experiments were performed over a single day, with a delay of roughly 6 hours between the two experiments. We attribute the wavenumber difference between these two acquisitions to environmental variations in the laboratory within the day.

Finally, we combined both fine tuning approaches to ensure mode-hope-free single-mode emission over a wide range of injection current. Figure 10 shows the emitted spectrum for different injected currents. For each current, the z-position of the CRIGF filter is finely tuned in order to minimize the voltage across the QCL, prior to recording the emission spectra, thus following as best as possible the same longitudinal mode along the way. We were thus able to achieve single-mode lasing over a large current span, larger than 50 mA, achieving continuous tuning of the emission wavelength over slightly more than 1 cm^{-1}, as depicted on Fig. 10. One single mode jump can be seen at 300 mA.

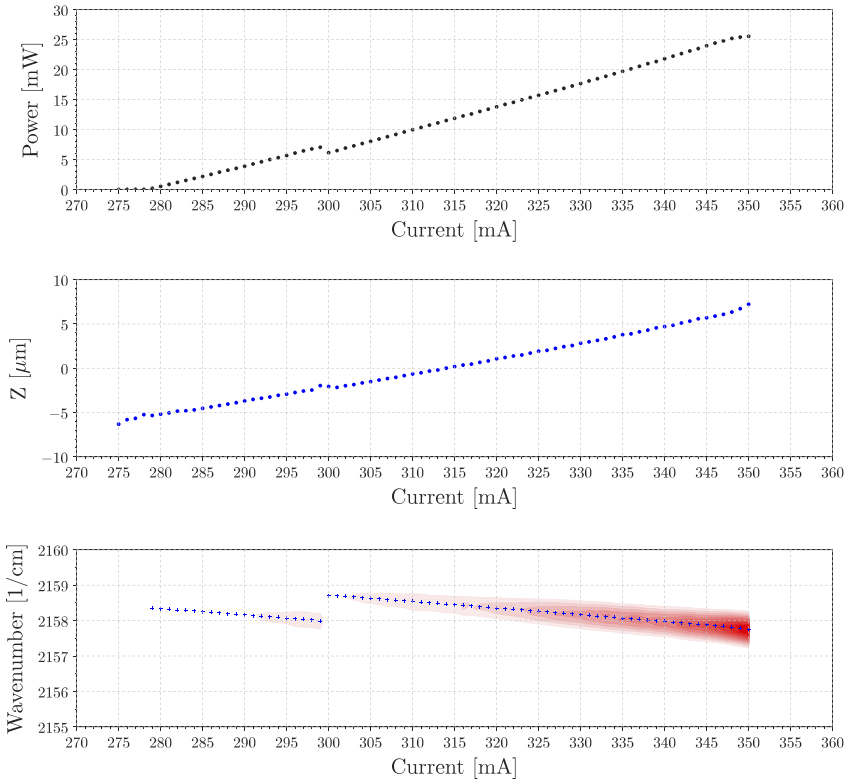

Fig. 10. Top : total emitted power versus injected current. Middle : variation of the Z position of the CRIGF for each current, with respect to its mean position. Bottom : emitted spectrum versus injected current in white to red linear color scale. The crosses correspond to the emission maximum.

Optics EXPRESS

5. Conclusion

We demonstrated wavelength stabilization of a QCL gain chip with a MIR CRIGF. The emission is single-mode, with fine and broadband tuning abilities. We demonstrated a short time wavelength stability and reproducibility better than 0.2 cm^{-1} despite the rather crude and unstable external cavity setup. A digital tuning range of 65 cm^{-1} was achieved with output powers in the range of 10 mW in continuous wave operation. This demonstration is a first step for implementation of CRIGF-based external cavity quantum cascade lasers as an alternative to more standard grating-based cavities. It may show interest in applications where continuous tuning is not required, but where wavelength stability and reproducibility are key.

Funding

Agence Nationale de la Recherche (ANR-14-ASTR-0024 (Calitrec project)).

Acknowledgments

Authors thankfully acknowledge the LAAS clean room team for technical support and technological expertise provided within the French RENATECH framework.

Disclosures

The authors declare no conflicts of interest.

References

1. A. Godard, "Infrared (2–12 μm) solid-state laser sources: a review," C. R. Phys. **8**(10), 1100–1128 (2007).
2. A. Hugi, R. Maulini, and J. Faist, "External cavity quantum cascade laser," Semicond. Sci. Technol. **25**(8), 083001 (2010).
3. K. Kintaka, T. Majima, J. Inoue, K. Hatanaka, J. Nishii, and S. Ura, "Cavity-resonator-integrated guided-mode resonance filter for aperture miniaturization," Opt. Express **20**(2), 1444 (2012).
4. X. Buet, E. Daran, D. Belharet, F. Lozes-Dupuy, A. Monmayrant, and O. Gauthier-Lafaye, "High angular tolerance and reflectivity with narrow bandwidth cavity-resonator-integrated guided-mode resonance filter," Opt. Express **20**(8), 9322–9327 (2012).
5. S. Augé, A. Monmayrant, S. Pelloquin, J. B. Doucet, and O. Gauthier-Lafaye, "Tunable graded cavity resonator integrated grating filters," Opt. Express **25**(11), 12415–12420 (2017).
6. X. Buet, A. Guelmami, A. Monmayrant, S. Calvez, C. Tourte, F. Lozes-Dupuy, and O. Gauthier-Lafaye, "Wavelength-stabilised external-cavity laser diode using cavity resonator integrated guided mode filter," Electron. Lett. **48**(25), 1619–1621 (2012).
7. X. Baillard, A. Gauguet, S. Bize, P. Lemonde, P. Laurent, A. Clairon, and P. Rosenbusch, "Interference-filter-stabilized external-cavity diode lasers," Opt. Commun. **266**(2), 609–613 (2006).
8. S. Augé, S. Gluchko, A. Fehrembach, E. Popov, T. Antoni, S. Pelloquin, A. Arnoult, A. Monmayrant, and O. Gauthier-Lafaye, "Mid-infrared cavity resonator integrated grating filters," Opt. Express **26**(21), 27014 (2018).
9. J. von Staden, T. Gensty, W. Elsäßer, G. Giuliani, and C. Mann, "Measurements of the α factor of a distributed-feedback quantum cascade laser by an optical feedback self-mixing technique," Opt. Lett. **31**(17), 2574 (2006).
10. K. Bertling, Y. L. Lim, T. Taimre, D. Indjin, P. Dean, R. Weih, S. Höfling, M. Kamp, M. von Edlinger, J. Koeth, and A. D. Rakić, "Demonstration of the self-mixing effect in interband cascade lasers," Appl. Phys. Lett. **103**(23), 231107 (2013).

147.94.134.17 (fs 2020-02-07 08:23:09)